Higher harmonic wave loads on structures under regular and irregular waves based on weak-scatterer theory

Xinmeng Zeng[1,2,*], Yanlin Shao[3], Guillaume Ducrozet[2], Florian Hulin[2], Xingya Feng[4], Kun Xu[1]

[1]Ocean University of China, Qingdao, China
[2]Nantes Université, École Centrale Nantes, CNRS, LHEEA, UMR 6598, Nantes, France
[3]Technical University of Denmark, Kgs. Lyngby, 2800, Denmark
[4]Southern University of Science and Technology, Shenzhen, China

[*]E-mail: xinmeng_zeng@163.com

1 INTRODUCTION

The weak-scatterer (WS) theory strategically retains fully nonlinear kinematics of the incident wave while neglecting the higher-order effects of scattered waves, thereby achieving an effective balance between capturing the "low-hanging" nonlinearities and maintaining numerical robustness. However, its ability to predict wave loads beyond second order may be limited when the neglected nonlinear scattered-wave effects become non-negligible. This study introduces two effective enhancements to the existing WS models: (i) a nonlinear waterline correction applied as a post-processing step to recover critical contributions omitted in the standard WS formulation, without changing the embeded boundary-value-problem solver; (ii) a Morison-type drag model based on the instantaneous Keulegan-Carpenter number to estimate important viscous-drag contributions for floating structures, such as those induced by damping plates. The enhanced numerical model is validated and its performance assessed for large-amplitude waves through established benchmark cases, including monopile foundations and the OC6 DeepCwind semi-submersible floater under both regular and irregular wave conditions. The model is implemented within a time-domain higher-order boundary element (HOBEM) solver, whose stability is substantially improved through the optimized weighted least-squares low-pass filter, which is applicable for unstructured meshes. It employs Stream function theory for regular incident waves and the open-source High-Order Spectral Numerical Wave Tank (HOS-NWT) for irregular, highly nonlinear incident waves. Our work delivers an enhanced numerical implementation of the WS framework that substantially extends its practical applicability.

2 THEORY

The kinematic and dynamic free surface conditions are linearized with respect to the incident wave position (η_I) using the first-order Taylor series expansion along the vertical direction. With a semi-Lagrangian description, the leading-order free surface conditions for the scattered quantities η_S and ϕ_S are defined on η_I as follows:

$$
\begin{cases}
\dfrac{\delta\eta_S}{\delta t} = \dfrac{\partial\phi_S}{\partial z} - \left(\dfrac{\partial\phi_I}{\partial x}\dfrac{\partial\eta_S}{\partial x} + \dfrac{\partial\phi_I}{\partial y}\dfrac{\partial\eta_S}{\partial y}\right) - \left(\dfrac{\partial\phi_S}{\partial x}\dfrac{\partial\eta_I}{\partial x} + \dfrac{\partial\phi_S}{\partial y}\dfrac{\partial\eta_I}{\partial y}\right) \underline{- \left(\dfrac{\partial\phi_S}{\partial x}\dfrac{\partial\eta_S}{\partial x} + \dfrac{\partial\phi_S}{\partial y}\dfrac{\partial\eta_S}{\partial y}\right)} \\
\qquad + \eta_S\left(\dfrac{\partial^2\phi_I}{\partial z^2} - \dfrac{\partial\eta_I}{\partial x}\dfrac{\partial^2\phi_I}{\partial x\partial z} - \dfrac{\partial\eta_I}{\partial y}\dfrac{\partial^2\phi_I}{\partial y\partial z}\right) \\
\dfrac{\delta\phi_S}{\delta t} = -g\eta_S + \dfrac{\partial\eta_I}{\partial t}\dfrac{\partial\phi_S}{\partial z} - \left(\dfrac{\partial\phi_I}{\partial x}\dfrac{\partial\phi_S}{\partial x} + \dfrac{\partial\phi_I}{\partial y}\dfrac{\partial\phi_S}{\partial y} + \dfrac{\partial\phi_I}{\partial z}\dfrac{\partial\phi_S}{\partial z}\right) \underline{- \frac{1}{2}\left(\dfrac{\partial\phi_S}{\partial x}\dfrac{\partial\phi_S}{\partial x} + \dfrac{\partial\phi_S}{\partial y}\dfrac{\partial\phi_S}{\partial y} + \dfrac{\partial\phi_S}{\partial z}\dfrac{\partial\phi_S}{\partial z}\right)} \\
\qquad - \eta_S\left(\dfrac{\partial^2\phi_I}{\partial z\partial t} + \dfrac{\partial\phi_I}{\partial x}\dfrac{\partial^2\phi_I}{\partial x\partial z} + \dfrac{\partial\phi_I}{\partial y}\dfrac{\partial^2\phi_I}{\partial y\partial z} + \dfrac{\partial\phi_I}{\partial z}\dfrac{\partial^2\phi_I}{\partial z^2}\right)
\end{cases}
\tag{1}
$$

Here, ϕ_I and η_I are $O(1)$, meaning that they are of the same order of magnitude as the characteristic structural dimensions, whereas ϕ_S and η_S are $O(\epsilon)$. The parameter ϵ is a non-dimensional quantity that characterizes the smallness of these terms.

The enhanced model will be denoted as WS-C, and the original model as WS-O. In Eq. (1), all terms are $O(\epsilon)$, with the exception of the underlined terms, which are $O(\epsilon^2)$. These $O(\epsilon^2)$ contributions are omitted in all existing WS formulations in the literature [1, 2]. In the present work, we also exclude them from the direct time integration of the free-surface boundary conditions to maintain the original WS framework. Instead, we introduce a simple post-processing correction that recovers key nonlinear contributions from these terms. This is achieved by performing a re-time-stepping procedure within the same time step, during which all forcing terms, including the $O(\epsilon^2)$ terms in Eqn (1) are retained. This yields updated values for η_S and ϕ_S, denoted as η_S^* and ϕ_S^*. These corrected variables, η_S^* and ϕ_S^*, are then used in place of η_S and ϕ_S when evaluating the two waterline integrals in Eq. (2) for wave load calculation. A further enhancement compared to the WS-O model is the inclusion of an additional $O(\epsilon^2)$ term in the hydrodynamic load simulation, as shown in underline term of Eq. (2). In the WS-C model, the i-th component of the hydrodynamic loads can be calculated as:

$$
\begin{aligned}
f^i_{\text{Hydro}} \approx & -\rho \iint_{S_B^{w_I}} \left(\phi_t + \frac{1}{2}|\nabla\phi|^2 + gz \right) n_i \, ds - \rho \oint_{\tau_I} \eta_S \left(\phi_t + \frac{1}{2}|\nabla\phi|^2 + g\eta_I \right) n_i \, dl \\
& - \rho \oint_{\tau_I} \frac{1}{2}\eta_S^2 \underline{\left(g + \frac{\partial^2\phi_I}{\partial z \partial t} + \frac{\partial\phi_I}{\partial x}\frac{\partial^2\phi_I}{\partial x \partial z} + \frac{\partial\phi_I}{\partial y}\frac{\partial^2\phi_I}{\partial y \partial z} + \frac{\partial\phi_I}{\partial z}\frac{\partial^2\phi_I}{\partial z^2} \right)} n_i \, dl
\end{aligned}
\tag{2}
$$

where $S_B^{w_I}$ is the wetted body surface under the incident wave profile. n_i is the i-th component of the normal vector on $S_B^{w_I}$. τ_I is the waterline of the structure defined as the intersection between the body surface and the incident wave surface, ϕ_t and $\nabla\phi$ include incident and scattered components.

We employ a HOBEM to solve the boundary value problem, time-integrated with a fourth-order Runge-Kutta (RK4) scheme. Solution stability is ensured through adaptive mesh assembly and a robust, tailored weighted least-squares low-pass filter [3]. Fig. 1 shows the numerical boundary-element model alongside the comparative experimental model.

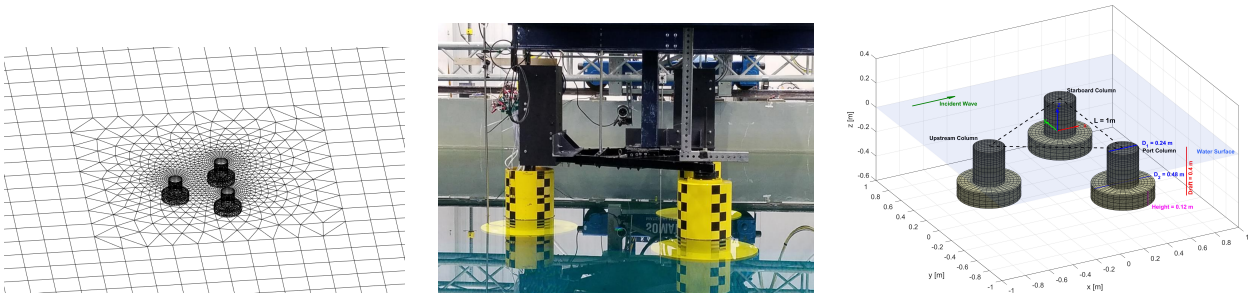

(a) Free surface mesh (b) Experimental model (c) Mesh model on structure

Figure 1: HOBEM and experimental model of the OC6 DeepCwind semi-submersible floater.

3 RESULTS

This section presents higher-harmonic wave loads on a monopile and a semi-submersible. As a start, we simulate wave diffraction of a monopile of radius R and consider a series of regular-wave cases reported in [4] and compare the results with fully nonlinear potential flow (FNPF) simulations based on immersed-boundary adaptive harmonic polynomial cell (IB-AHPC) method [1], experimental data and FNV theory [4] to evaluate the WS models' ability to capture first- to

third-harmonic wave loads. To demonstrate the capability of the WS-C model, the case examines a fixed wavelength ($kR = 0.182$) and relative depth $h/R = 5.51$, with varying wave steepness kA^1, A^1 is the linear wave amplitude.

Fig. 2 illustrates the normalized harmonic amplitudes as a function of kA^1. For $kA^1 \leq 0.1$, both WS-O and WS-C models show good agreement with experimental data and FNPF results for the first- to third-harmonic wave loads. When $kA^1 > 0.1$, the WS-O model begins to overestimate the third harmonic load, and a slight overestimation of the second harmonic is also observed compared to experimental results for $kA^1 > 0.13$. When $kA^1 > 0.18$, the second and third harmonics of WS-O prediction significantly deviate from the other results and tend to become nonphysical. However, the WS-C model shows consistently good trend of the second harmonics and reasonably good third harmonics compared with the experiments and the FNV model. By employing an optimized WLS filtering strategy [3], the present implementation of the WS theory successfully overcomes the limitation of previous models [1, 2] in handling cases with stronger nonlinearities, enabling stable computation up to $kA^1 = 0.25$ at least, thereby reaching the nonlinear regime where significant ringing effects are reported to be excited.

Although over-estimations persist in comparison to model tests, the WS-C model shows much smaller over-estimations than the FNV theory for large kA, indicating its improved performance in steep waves. The WS model sacrifices some of the higher-order nonlinear interactions in exchange for numerical robustness, which, however, makes it suitable for engineering applications while still capturing essential nonlinear phenomena. In summary, the WS-C model accurately predicts harmonic wave loads under weakly nonlinear conditions ($kA^1 \leq 0.1$). Under stronger nonlinearity ($kA^1 > 0.1$), it overestimates the second and third harmonics, yet these deviations remain within acceptable margins relative to the FNV theory for engineering practice. Neglecting the ϵ^2 terms in the free-surface boundary conditions yields a negligible discrepancy in the predicted loads under conditions of weak nonlinearity ($kA^1 < 0.13$). However, as kA increases, this simplification results in a non-negligible over-prediction in the second- and third-harmonic loads compared to the model that retains these terms, while the first-order component remains unaffected.

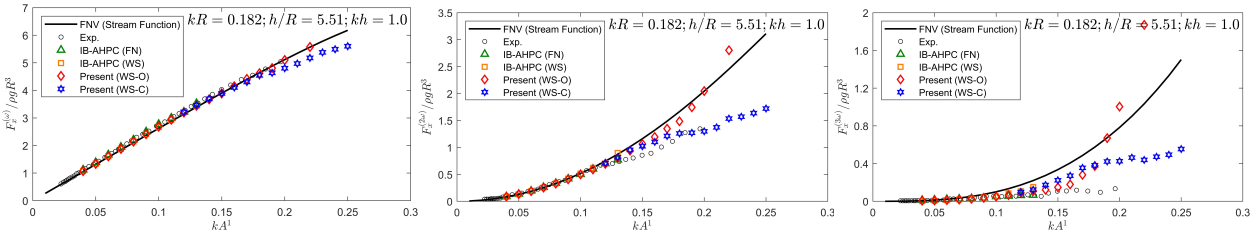

(a) First harmonics (b) Second harmonics (c) Third harmonics

Figure 2: Comparison of the normalized amplitudes for the (a) first, (b) second, and (c) third harmonics of the horizontal wave force as a function of kA^1 between the present model and existing experimental, numerical, and FNV model for $kR = 0.182$ and $h/R = 5.51$.

In the next step, we aim to validate the hydrodynamic loads on the sub-components of a floater using the WS solver. The OC6 DeepCwind experimental campaign is used to assess wave loads on substructure components. Another purpose of this validation is to demonstrate the effectiveness of the Morison-type drag model based on instantaneous KC values for the heave plates.

To empirically account for the viscous loads on the heave plates in the present potential-flow-based time-domain simulations, the Morison-type drag loads on the damping plates are included. The drag coefficient C_d is formulated as a function of the local KC number, typically established via forced oscillation CFD simulations or experimental measurements. Instantaneous KC values for

each structural member must be evaluated in each time step according to the local flow field. The instantaneous drag coefficient C_d is subsequently obtained from the predefined C_d(KC) function or the tabulated C_d-KC database, where KC is defined as $\frac{v_{\max}T}{D}$. In a more general case with floating structures in irregular waves, KC could be estimated using the nearest available time history of the relative velocity between the heave plate and the ambient flow, the instantaneous KC values are estimated for the horizontal pontoons of the FOWT, where T is taken as the local zero-uncrossing period, and $v_{\max}$ as the magnitude of the maximum or minimum relative velocity from the immediate previous oscillatory cycle. Fig. 3 compares the simulated and measured time histories of hydrodynamic loads on different columns with kA^1=0.1023. The numerical results of the surge force on the upstream and starboard columns agree well with the experiments. For the heave force on the upstream column, however, the potential-flow simulation without drag loads underestimates the measurements. This discrepancy is significantly reduced by incorporating the Morison model to account for viscous effects. Similarly, the prediction of pitch moment is clearly improved with the inclusion of the Morison model. The improvements account for 16.8% of the total heave force and 26% of the pitch moment on the upstream column. For the downstream column, the potential flow results align well with the experimental data. The addition of the Morison model has a minor influence on the heave force but slightly increases the pitch moment at the wave trough, which may be due to the wave scattering and interactions. For the same structures in irregular waves, more results will be presented at the workshop.

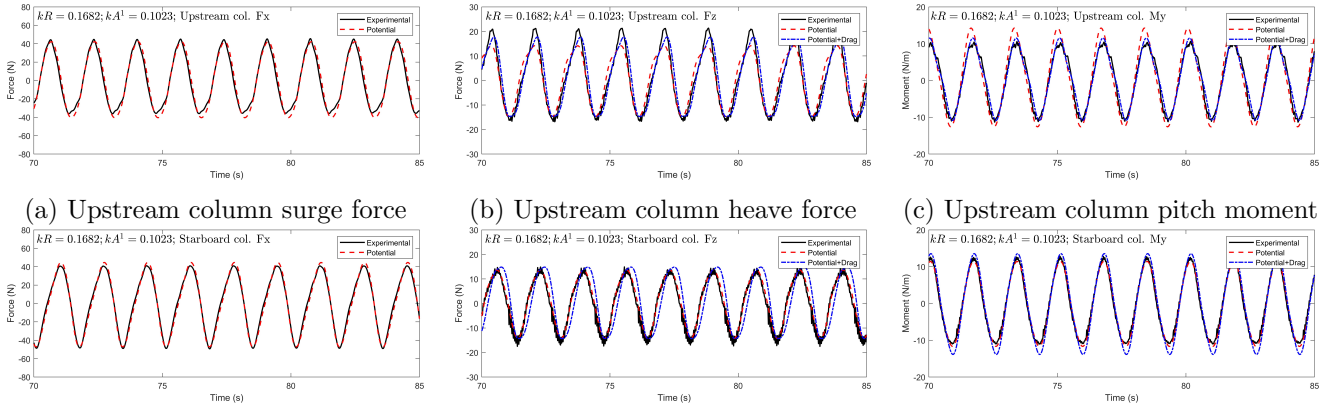

(a) Upstream column surge force (b) Upstream column heave force (c) Upstream column pitch moment

(d) Starboard column surge force (e) Starboard column heave force (f) Starboard column pitch moment

Figure 3: Wave-load time series on floater substructures with kA^1=0.1023: a comparison of experimental results and potential flow simulations with and without Morison drag correction.

REFERENCES

[1] Tong, C., Shao, Y., Bingham, H. B., and Hanssen, F.-C. W. 2024. *An adaptive harmonic polynomial cell method for three-dimensional fully nonlinear wave-structure interaction with immersed boundaries.* Physics of Fluids 36(3).

[2] Zhang, Y., and Teng, B. 2021. *A nonlinear potential flow model for higher-harmonic wave loads and ringing response of a monopile. Ocean Engineering 222*, 108574.

[3] Shao, Y., Zheng, Z., Liang, H., and Chen, J. 2022. *A consistent second-order hydrodynamic model in the time domain for floating structures with large horizontal motions.* Computer-Aided Civil and Infrastructure Engineering 37(7), 894–914.

[4] Kristiansen, T., and Faltinsen, O. M. 2017. *Higher harmonic wave loads on a vertical cylinder in finite water depth. Journal of Fluid Mechanics 833*, 773–805.